

Supporting Information

A Reassessment of the Electronic Structure of Cr(VI) Sites Supported on Amorphous Silica and Implications for Cr Coordination Number.

Nathan M. Peek[§], David B. Jeffcoat[§], Cristina Moisii[†], Lambertus van de Burgt[§], Salvatore Profeta, Jr.[§], Susannah L. Scott[‡], A. E. Stiegman^{§*}

[§]Department of Chemistry and Biochemistry, Florida State University, Tallahassee, FL 32306

[†]Department of Science, Engineering & PE, Eastern Florida State College, Cocoa, FL 32922

[‡]Department of Chemical Engineering, University of California, Santa Barbara, CA 93106

* To whom correspondence should be addressed. Email: Stiegman@chem.fsu.edu

Experimental Procedures

Xerogel Synthesis and Silica Monolith Fabrication. Cr/SiO₂ xerogel monoliths and disks were made by adapting a previously published technique.¹⁻³ Sols were made by the addition of an alcoholic solution of tetramethylorthosilicate (TMOS, Gelest) and the desired quantity of chromic acid to a water/2-propanol mixture. The stock solution of chromic acid was made using CrO₃ (99.9 %, Aldrich) and deionized water (10⁻¹⁸ W; Barnsted E-Pure system). In order to obtain homogeneous mixtures, all solutions were sonicated for 5 min. For the monoliths, four mL aliquots of the sol were dispensed into 1 cm styrene cuvettes, sealed and allowed to gel. Disks were made by adding two mL aliquots of the sol to micro-sized hinged-lid lab vials (Lacontainerstore). The caps were removed after gelation and the materials were allowed to age and evaporate for 3–4 months. The samples were then dried in air in a programmable furnace. The temperature was initially ramped to 100 °C at a rate of 0.5 °C/h and held for 72 h. It was then ramped at the same rate to 500 °C, where it was maintained for 36 h. Finally, the samples were cooled back to room temperature over a period of 95 h. The resulting materials were transparent monoliths of dimension ca. 0.5 x 0.5 x 1.5 cm, or disks of 0.18 cm thickness x 0.8 cm diameter, containing from 0.005 to 3.0 mol% Cr [mol Cr/(mol Cr+mol Si) x 100 %].

Sample Preparation. All samples were calcined in a tube furnace in open air at 500 °C for 12 h prior to experiments. The samples were flushed with ultra-high-purity nitrogen or argon before being loaded into an argon-filled glove box. All gases used were UHP grade from Airgas.

UV-vis Spectroscopy. UV-visible spectra were collected on a Perkin-Elmer Lambda 900 spectrophotometer in transmission mode, with the beam passing through the Cr/SiO₂ sol-gel. The spectra were collected through a sealed, high-temperature/high-pressure (HTHP) spectroscopic cell (International Crystal Laboratories) equipped with sapphire windows. A metal block installed in the bottom of the sample chamber in the UV-vis spectrophotometer is designed to hold the HTHP cell in place so that the light beam goes directly through the sample. Prior to each experiment, a blank spectrum was collected using the empty HTHP cell under vacuum. In an argon-filled glove box, a freshly calcined 0.005% Cr/SiO₂ xerogel disk was loaded into the HTHP cell and sealed. After the cell was removed from the glove box, it was connected to a vacuum line, evacuated for 10 min, then installed in the UV-vis spectrophotometer for spectrum collection.

Fluorescence Spectroscopy. Fluorescence spectra were collected on a Spex Fluorolog II equipped with 0.22 m double monochromators (Spex 1680) and a 450 W Hg/Xe lamp. All emission and emission excitation experiments were performed using 0.005% Cr/SiO₂ sol-gel monoliths. Right angle collection was used for both emission and emission excitation spectra and cutoff filters were utilized for suppressing second-order excitation lines. Room temperature spectra were collected in a quartz cell specially designed for spectroscopic studies. It is equipped with a cylindrical reaction container for high temperature treatments, and a side-arm with a 5 mm-square quartz fluorescence cell, into which the monolith can be transferred for spectroscopic measurements without exposure to the laboratory ambient. For low temperature studies, samples were mounted on an APD Model DE-202 cryo-stat, shrouded, and evacuated. The cryo-stat's temperature can be controlled from 10 K to room temperature. Samples were carefully aligned to maximize intensity in the detector prior to collection of spectra to ensure reproducible emission intensities. All reported spectra were corrected for the lamp profile and the detector response. Emission spectra reported in wavenumber units were corrected in the standard way for the bandpass variability in spectra collected at fixed wavelength resolution. Emission spectra

were collected by exciting at 350 nm. The emission excitation spectra were collected by monitoring at 610 nm with a bandpass of 2.13 nm for both.

Fluorescence anisotropy experiments were performed on the instrument described above, and in the quartz cell. Two Glan-Thompson polarizers were inserted into the beam path in the L-format. The anisotropy was determined by collecting four spectra and applying the following equation:

$$r = \frac{I_{vv} - GI_{vH}}{I_{vv} + 2GI_{vH}} \quad (\text{S1})$$

where $G = I_{HV} / I_{HH}$. In eq S1, r is the polarization anisotropy, I is the emission intensity, and the

subscripts v and h indicate the position of the polarizers (the first indicates the position of the excitation polarizer, and the second the position of the emission polarizer).⁴ The emission was monitored at 610 nm at room temperature for a 0.005% Cr/SiO₂ monolith under vacuum.

Emission lifetime measurements. Lifetime measurements were obtained using a Transient Absorption Spectrometer consisting of an Edinburgh Instruments LP980-KS Laser Flash Photolysis Spectrometer and a Continuum Horizon II Optical Parametric Oscillator (OPO) pumped by a Continuum Surelite EX Nd:YAG laser. The Edinburgh Instruments LP980-KS spectrometer is capable of measuring laser-induced transient absorption and emission kinetics and spectra on time scales as short as 10 ns. The spectrometer uses laser pulses from a Continuum Nd:YAG/OPO laser system as a pump source.

The Continuum Surelite EX Nd:YAG laser is an oscillator-only laser optimized for 10 Hz operation and equipped with 2nd and 3rd harmonic nonlinear crystals to emit combined 1064, 532 and 355 nm pulses. The Surelite EX pumps a Continuum mid-band OPO using 355 nm pulses attenuated to a maximum of 225 mJ/pulse to allow automated wavelength selection in the 400-2750 nm range (Signal/Idler) using two coupled BBO crystals. The wavelength range is extended to 192-400 nm using two more BBO crystals to mix the OPO Signal with residual 1064 nm fundamental and/or generate the 2nd harmonic. Wavelength selection is controlled by Continuum software "Horizon". The Continuum system pulse rate and Q-switch delay are controlled by the spectrometer software "L900". OPO typical output is 3-5 ns with 3-7 cm⁻¹ linewidth.

The signals to be measured are dispersed through a 300 mm focal length Czerny-Turner monochromator (TMS302-A, F/4.1) equipped with a three grating turret. Dispersed light is directed to either an intensified CCD (iCCD) camera (Andor iStar DH 320T-25F-03-812) or a detector. The Andor iCCD camera consists of a Peltier-cooled (to -200 °C) 1024x256 array of 26 μm pixels equipped with a 25-mm image intensifier which allows a minimum optical gate width of 7 ns (the L900 software limits the gate to 10 ns). Using a 150 groove/mm grating optimized at 500 nm, the iCCD camera covers a 540 nm spectral area in the 200-900 nm wavelength range. The second exit port accommodates one of three single wavelength detectors for recording kinetic data. The first detector is a photomultiplier tube (PMT, Hamamatsu R928) wired for high light conditions using 5 of the 9 dynode stages. The amplifier circuitry allows either fast response time (1 ns) for recording transients up to ~100 μs or increased signal by increasing the impedance (and increasing the response time) for recording longer-lived transients. The PMT covers the 185-870 nm spectral range and uses an 1800 groove/mm grating optimized at 500 nm. The second detector is an InGaAs photodiode detector (PD, Hamamatsu G12180-230A)

operating in the near-infrared from 900 to 1650 nm with a response width of 100 ns. The PD uses a 600 groove/mm grating optimized at 1 μm . The third detector is similar to the first in that it uses a similar PMT (Hamamatsu R928) but is optimized for low light conditions by wiring all 9 dynodes and operating in photon-counting mode with Multi Channel-Scaling (MCS). The PMT uses the same grating as the first detector. The first two detectors use a Tektronix digital storage oscilloscope (TDS3012C, 100 MHz bandwidth, 1.25 GHz sampling rate) to record and digitize the transient signals.

The LP980-KS spectrometer can be operated in four modes, Kinetic Emission, Kinetic Absorption, Spectral Emission and Spectral Absorption. All aspects of the instrument except OPO wavelength selection are fully automated using the L900 software.

Kinetic emission spectra were collected at both room temperature and 77 K. For both studies, the sample holders used were those described above for fluorescence spectroscopy. Samples were excited at 450 nm while detecting at 626 nm with a bandpass of 20 nm. The study was performed on a 0.005% Cr/SiO₂ monolith.

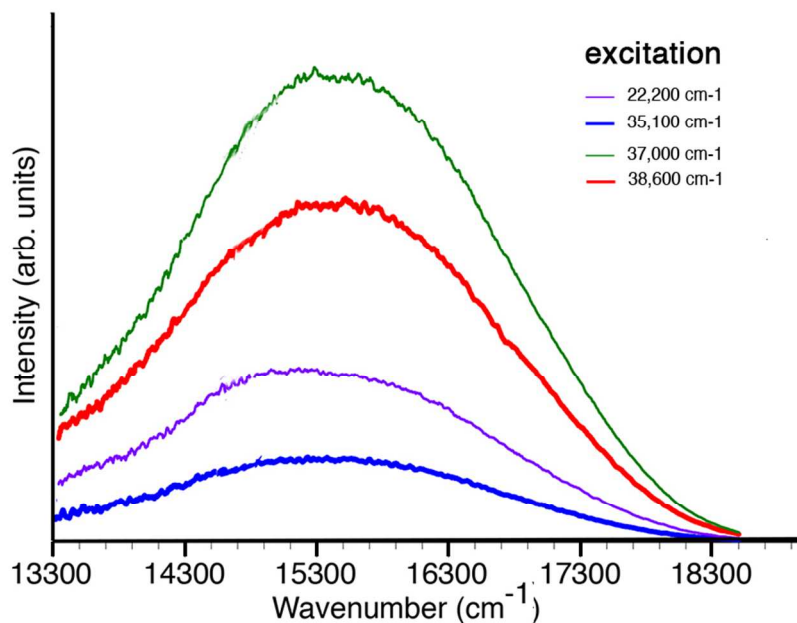


Figure S1. Emission spectra of a 0.005 mol % Cr(VI)/SiO₂ xerogel, collected at 77 K for different excitation wavelengths.

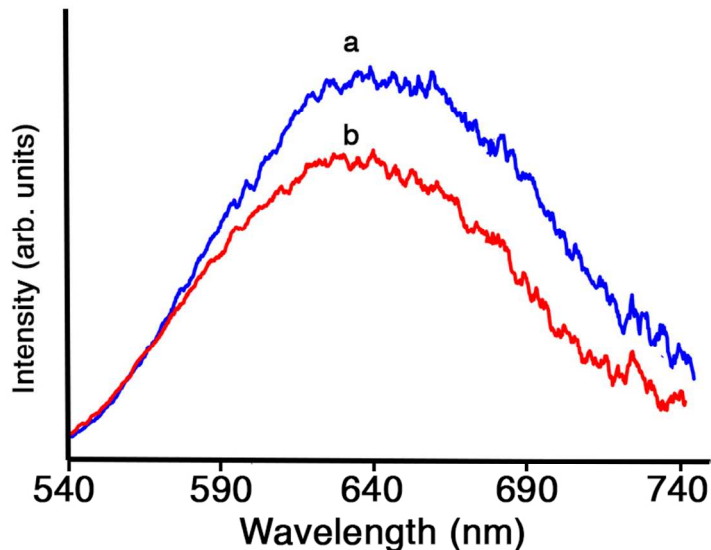


Figure S2. Emission spectrum from a 0.005 mol % Cr(VI)/SiO₂, recorded (a) in vacuum, and (b) under O₂.

Electronic Structure Calculations

Avogadro. Molecules were initially built in Avogadro^{(1),5} a cross-platform molecular editing software, due to the easy-to-use interface and ability to optimize the geometry through energy minimization. This first optimization is a relatively quick calculation using force fields formed with a molecular mechanics simulation. Minimization requires a function, provided by the force fields, as well as a starting guess or set of coordinates that can easily be built in this program. However, care must be taken with larger molecules when first building the skeleton structure because a bad starting point will ruin further optimization attempts. The magnitude of the first derivative can be used to determine the direction and magnitude of a step, or the change in coordinates, required to approach a minimum configuration for the geometry. The magnitude of the first derivative is also a rigorous way to characterize convergence. A minimum has converged when the derivatives are close enough to zero. The default tolerance in Avogadro is 10⁻⁸ kJ/mol. To reach the minimum, the structure must be successively updated by changing the coordinates (i.e., taking a step) and checking for convergence. Each complete cycle of differentiation and stepping is known as a minimization iteration, and typically thousands of iterations are required for these monomers and polymers to reach convergence. There are two reasons we used Avogadro to build molecules over Spartan16: you can watch the energy minimization in real time using Avogadro to be more certain that the resulting geometry will not fail in further computations, and the molecular mechanics simulations are a lower level of theory, but it's a good idea to work your way up the theory ladder by providing better initial guesses to reduce the possibility of failure at higher levels of theory.

Avogadro can output .pdb (Protein Data Bank) files that contain the Cartesian coordinate information that can be read into Spartan '16. There is also the option of copying the coordinates through the programs Cartesian Editor and importing this into the Gaussian '09 .com files.

Gaussian09⁶ computations involved optimizing all structures using the B3LYP functional with a triple-zeta basis set, 6-311G*. This optimization is imported into Avogadro using the .log files output by Gaussian09. The optimized structure is displayed in Avogadro along with all the vibrational modes calculated. Furthermore, we could select specific modes and have an animation show us what specific bond stretches and movements were present in each mode based on the Gaussian09 output. Having this to compare to similar vibrational mode output from VIBRATZ and Spartan16 helped ensure no miscalculations occurred between the various programs.

Spartan16. Developed by Wavefunction, Spartan16 was used to perform density functional theory calculations on ground-state molecules. It will output the symmetry of the molecule, the thermodynamics, and the HOMO-LUMO gap along with values for adjacent energy states. For model I, we constrained the symmetry to C_{2v} , and the ability to use keyword in Spartan16 to keep this constraint active throughout the DFT calculations proved very useful.

Gaussian 09. Gaussian09 is an electronic structure modeling software program run on the High-Performance Computing Cluster located at the Research Computing Center on the Florida State University campus. A properly formatted input file (.com) is needed to submit the computational job alongside a command file (.cmd) formatted to follow SLURM submission rules which specifies parameters such as job title, memory usage, and maximum run time. Gaussian09 and Spartan16 both perform DFT calculations, but the Spartan16 program is run on a single lab computer. Therefore, Gaussian 09 was the initial program due to improved computational time; Spartan16 output is employed as a reference to compare the results to.

We ran DFT calculations using the B3LYP hybrid functional with a 6-311G* basis set for all computations. The first computations involved optimizing the input geometry under these set conditions and then determining spectral frequencies. Using specific keywords, the output file (.log) was set to contain frequency values related to all normal modes of the optimized structure as well as the relative IR and Raman intensities at each mode. If any imaginary frequencies ever appeared, the coordinates for the initial structure would be reassessed and/or the convergence criteria would be loosen from default values.

B3LYP and 6-311G (used in Gaussian and Spartan).* The B3LYP hybrid functional was used with a 6-311G* basis set for all DFT computations.⁷ The B3LYP (Becke, 3-parameter, Lee-Yang-Parr)⁸ exchange-correlation functional is considered a hybrid functional because it incorporates a portion of the exact exchange calculated by Hartree-Fock theory with exchange and correlation values from either *ab initio* or empirical sources. It is also termed an implicit density functional for relying on the electron density and not representing the exact exchange energy values. This hybrid approach provides a simple scheme for improving many molecules properties that tend to be poorly described with simple *ab initio* functionals: atomization energies, bond lengths, and vibration frequencies.

The basis set 6-311G* is a valence triple-zeta polarized Pople basis set.⁹ We decided to use a triple-zeta basis set because chromium is a heavy metal element and one of the last ones to be described by Pople basis sets when you consider polarization functions.¹⁰ Increasing the number of Slater-type orbitals has been shown to improve computations involving heavy metal atoms.¹¹

The B3LYP functional has been documented to describe heavy metal complexes adequately, but the need to calculate dozens of excited states above the ground state required that other functionals be considered. Long-range correlated functionals follow the same hybrid functional structure as B3LYP but have been shown to solve various DFT problems that have never been solved by other functionals, including the accurate representation of remote excited states.¹² The long-range ω B97X functional was suggested to our group. The excitation energies in Tables S1 and S2 compare the computational results for the hybrid functionals applied to the Cr(VI) models **I** and **II**.

Table S1. Effect of DFT functional on computed transition energies (TD-DFT at 6-311G*) for model **I**

Observed (cm ⁻¹)	Calculated (cm ⁻¹)	
	B3LYP	ω B97X
22,800	24,300	24,706
29,100	30,500	30,651
36,900	36,681	39,644
41,500	42,798	44,386

Table S2. Effect of DFT functional on computed transition energies (TD-DFT at 6-311G*) for model **II**

Observed (cm ⁻¹)	Calculated (cm ⁻¹)	
	B3LYP	ω B97X
22,800	24,640	27,320
29,100	29,998	32,940
36,900	35,983	39,180
41,500	41,559	42,004

Computed electronic transitions for model **I** are comparable for all excited states with both functionals. However, computed electronic transitions for model **II** are in better agreement with the B3LYP values for the lower energy excited states, while ω B97x begins to converge to the spectroscopic values at higher excited states, as expected for a long-range correlated functional. It is worth noting that the final geometry outputs as well as the excited state symmetries are identical for both functionals.

Ultimately, the data presented in this paper (with the exception of Table S2) were obtained using the B3LYP functional, due to the anomalous HOMO-LUMO gap energies reported in Spartan16 and Gaussian09 for the ω B97x functional. These programs gave a HOMO-LUMO gap ca. 4.3 eV for model **I** using B3LYP, but the gap more than doubled to 10.3 eV using ω B97x. Nothing even close to that value has ever been reported or considered accurate.¹³

Chemission. This program takes the .log output files from Gaussian09 TD-DFT calculations. Remember that the main output is the energy values for the number of states that you specify along with oscillator strength. Chemission gives a breakdown of the contributions to each energy state that come from electrons moving from state to state. This information is already given in the .log file, but it is formatted horribly with no graphics to show the HOMO and LUMO states. Chemission does a much better job of providing spectra, graphics, and

models based on the TD-DFT computations. Also, Chemissian has the capability to describe and plot the Natural Transition Orbitals (NTO).

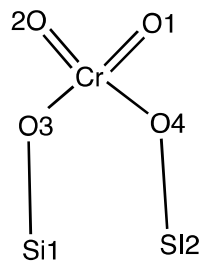


Figure S3. Atom numbering scheme for models **I**, **II** and **III**.

Table S3. Calculated bond lengths (Å) and angles (°) for dioxoCr(VI) models

	I	II	III
Bond			
Cr=O1	1.5608	1.5546	1.5599
Cr=O2	1.5608	1.5529	1.5597
Cr-O3	1.7492	1.7433	1.7468
Cr-O4	1.7492	1.7489	1.7587
Si1-O3	1.6523	1.6612	1.6629
Si2-O4	1.6523	1.6683	1.7527
Angle			
O1=Cr=O2	109.08	109.88	109.22
O3-Cr-O4	103.81	101.76	109.30
O3-Cr=O2	110.97	111.14	110.21
O4-Cr=O1	110.97	110.85	108.68
O3-Cr=O1	110.97	111.58	109.11
O4-Cr=O2	110.97	111.16	110.30
Si1-O3-Cr	132.95	131.16	131.13
Si2-O4-Cr	132.95	131.46	140.26

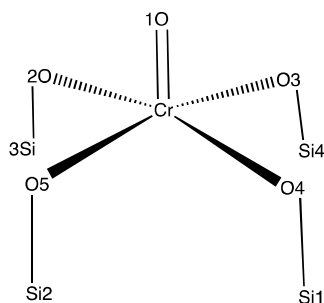


Figure S4. Atom numbering scheme for model **IV**

Table S4. Calculated bond lengths and angles for model **IV**

	Length (Å)		Angle (°)
Cr=O1	1.5383	4O-Cr=O1	107.24
Cr-O4	1.8229	3O-Cr=O1	107.17
Cr-O3	1.8192	2O-Cr=O1	107.27
Cr-O2	1.8209	5O-Cr=O1	107.20
Cr-O5	1.8185	1Si-O4-Cr	118.92
1Si-O4	1.6638	4Si-O3-Cr	119.05
4Si-O3	1.6651	3Si-O2-Cr	118.95
3Si-O2	1.6638	2Si-O5-Cr	118.96
2Si-O5	1.6655	2O-Cr-O4	145.49
		3O-Cr-O5	145.62

Table S5. Computed electronic transitions for model I

Transition Energy (cm ⁻¹)	One-Electron Promotions	Partial Transition Coefficients	Intensity f
24,342	HOMO \leftrightarrow LUMO	0.90	0.0015
	HOMO-2 \leftrightarrow LUMO	0.39	
	HOMO-3 \leftrightarrow LUMO+1	-0.14	
30,536	HOMO-3 \leftrightarrow LUMO	0.92	0.0125
	HOMO \leftrightarrow LUMO+1	0.23	
	HOMO-2 \leftrightarrow LUMO+1	0.17	
36,433	HOMO-2 \leftrightarrow LUMO+1	0.83	0.0058
	HOMO \leftrightarrow LUMO+1	-0.40	
	HOMO-9 \leftrightarrow LUMO+1	0.2	
	HOMO-4 \leftrightarrow LUMO+1	-0.18	
36,681	HOMO-1 \leftrightarrow LUMO+1	0.62	0.0317
	HOMO-6 \leftrightarrow LUMO	-0.62	
	HOMO-3 \leftrightarrow LUMO+2	-0.42	
	HOMO-12 \leftrightarrow LUMO	-0.16	
42,380	HOMO-8 \leftrightarrow LUMO	0.66	0.0800
	HOMO-12 \leftrightarrow LUMO	0.58	
	HOMO-5 \leftrightarrow LUMO+1	-0.21	
42,799	HOMO-13 \leftrightarrow LUMO	0.76	0.0051
	HOMO-11 \leftrightarrow LUMO	0.37	
	HOMO-4 \leftrightarrow LUMO+1	0.31	
	HOMO-6 \leftrightarrow LUMO+2	0.22	

Table S6. Computed electronic transitions for model **II**

Transition Energy (cm ⁻¹)	One-Electron Promotions	Partial Transition Coefficients	Intensity f
24,640	HOMO \leftrightarrow LUMO	0.96	0.0012
	HOMO-3 \leftrightarrow LUMO	-0.17	
	HOMO-4 \leftrightarrow LUMO+1	0.10	
29,998	HOMO-4 \leftrightarrow LUMO	0.63	0.0115
	HOMO-5 \leftrightarrow LUMO	0.44	
	HOMO-3 \leftrightarrow LUMO	-0.39	
	HOMO-2 \leftrightarrow LUMO	0.29	
35,982	HOMO \leftrightarrow LUMO+2	0.54	0.0117
	HOMO-3 \leftrightarrow LUMO+1	-0.39	
	HOMO-2 \leftrightarrow LUMO+1	-0.36	
41,558	HOMO-14 \leftrightarrow LUMO	0.44	0.0054
	HOMO-7 \leftrightarrow LUMO+1	0.42	
	HOMO-5 \leftrightarrow LUMO+1	-0.35	

Table S7. Computed electronic transitions for model **III**

Transition Energy (cm ⁻¹)	One-Electron Promotions	Partial Transition Coefficients	Intensity f
26,820	HOMO-3 \leftrightarrow LUMO	0.87	0.0016
	HOMO-3 \leftrightarrow LUMO+1	-0.26	
	HOMO-4 \leftrightarrow LUMO	0.23	
31,783	HOMO-1 \leftrightarrow LUMO	0.48	0.0216
	HOMO-12 \leftrightarrow LUMO	-0.35	
	HOMO-6 \leftrightarrow LUMO	-0.35	
	HOMO-8 \leftrightarrow LUMO	-0.35	
36,896	HOMO-9 \leftrightarrow LUMO	0.38	0.0059
	HOMO-6 \leftrightarrow LUMO	0.31	
	HOMO-4 \leftrightarrow LUMO	0.30	
40,254	HOMO-12 \leftrightarrow LUMO	0.46	0.0054
	HOMO-5 \leftrightarrow LUMO+1	0.42	
	HOMO-4 \leftrightarrow LUMO+1	-0.32	

Table S8. Computed electronic transitions for model IV

Transition Energy (cm ⁻¹)	One-Electron Promotions	Partial Transition Coefficients	Intensity f
23,338	HOMO-4 \leftrightarrow LUMO	0.82	0.0084
	HOMO-2 \leftrightarrow LUMO	0.30	
	HOMO \leftrightarrow LUMO+2	-0.26	
23,357	HOMO-5 \leftrightarrow LUMO	0.82	0.0080
	HOMO-1 \leftrightarrow LUMO	-0.30	
	HOMO \leftrightarrow LUMO+1	0.26	
32,178	HOMO-11 \leftrightarrow LUMO	0.88	0.0087
	HOMO-4 \leftrightarrow LUMO+2	0.19	
	HOMO-5 \leftrightarrow LUMO+1	0.19	
	HOMO-7 \leftrightarrow LUMO+4	0.16	
37,434	HOMO-7 \leftrightarrow LUMO+1	0.52	0.0190
	HOMO-8 \leftrightarrow LUMO+1	-0.46	
	HOMO-18 \leftrightarrow LUMO	0.36	
40,583	HOMO-5 \leftrightarrow LUMO+2	0.44	0.0548
	HOMO-6 \leftrightarrow LUMO+1	0.43	
	HOMO-5 \leftrightarrow LUMO+1	0.35	
	HOMO-6 \leftrightarrow LUMO+2	-0.35	

Additional References

References

1. Stiegman, A. E.; Eckert, H.; Plett, G.; Kim, S. S.; Anderson, M.; Yavrouian, A., Vanadia silica xerogels and nanocomposites. *Chem. Mater.* **1993**, *5*, 1591-1594.
2. Curran, M. D.; Gedris, T. E.; Stiegman, A. E.; Plett, G. A., Synthetic control over the production of multicomponent sol-gel materials: Fabrication of homogeneous vanadia-silica xerogels with high vanadium content. *Chem. Mater.* **1999**, *11*, 1120-1127.
3. Moisii, C.; Deguns, E. W.; Lita, A.; Callahan, S. D.; van de Burgt, L. J.; Magana, D.; Stiegman, A. E., Coordination environment and vibrational spectroscopy of Cr(VI) sites supported on amorphous silica. *Chem. Mater.* **2006**, *18*, 3965-3975.
4. Lakowicz, J. R., *Principles of Fluorescence Spectroscopy*; Springer: New York, 2006.
5. Hanwell, M. D.; Curtis, D. E.; Lonie, D. C.; Vandermeersch, T.; Zurek, E.; Hutchison, G. R., Avogadro: An advanced semantic chemical editor, visualization, and analysis platform. *J. Cheminformatics* **2012**, *4*.

6. Gaussian 09, REvision A.02 M. J. Frisch, G. W. T., H. B. Schlegel, G. E. Scuseria, M. A. Robb, J. R. Cheeseman, G. Scalmani, V. Barone, G. A. Petersson, H. Nakatsuji, X. Li, M. Caricato, A. Marenich, J. Bloino, B. G. Janesko, R. Gomperts, B. Mennucci, H. P. Hratchian, J. V. Ortiz, A. F. Izmaylov, J. L. Sonnenberg, D. Williams-Young, F. Ding, F. Lipparini, F. Egidi, J. Goings, B. Peng, A. Petrone, T. Henderson, D. Ranasinghe, V. G. Zakrzewski, J. Gao, N. Rega, G. Zheng, W. Liang, M. Hada, M. Ehara, K. Toyota, R. Fukuda, J. Hasegawa, M. Ishida, T. Nakajima, Y. Honda, O. Kitao, H. Nakai, T. Vreven, K. Throssell, J. A. Montgomery, Jr., J. E. Peralta, F. Ogliaro, M. Bearpark, J. J. Heyd, E. Brothers, K. N. Kudin, V. N. Staroverov, T. Keith, R. Kobayashi, J. Normand, K. Raghavachari, A. Rendell, J. C. Burant, S. S. Iyengar, J. Tomasi, M. Cossi, J. M. Millam, M. Klene, C. Adamo, R. Cammi, J. W. Ochterski, R. L. Martin, K. Morokuma, O. Farkas, J. B. Foresman, and D. J. Fox, Gaussian Inc. Wallingford, CT, 2016.
7. Dreizler, R. M.; Gross, E. K. U., *Density Functional Theory*; Springer: Berlin, 1990.
8. Miehlich, B.; Savin, A.; Stoll, H.; Preuss, H., Results obtained with the correlation-energy density functionals of Becke and Lee, Yang and Parr. *Chem. Phys. Lett.* **1989**, *157*, 200-206.
9. Krishnan, R.; Binkley, J. S.; Seeger, R.; Pople, J. A., Self-consistent molecular-orbital methods .20. basis set for correlated wave-functions. *J. Chem. Phys.* **1980**, *72*, 650-654.
10. Hehre, W. J.; Radom, L.; Schyler, P. v. R.; Pople, J. A., *AB INITIO Molecular Orbital Theory*; Wiley: New York, 1986.
11. Huzinaga, S., Basis-sets for molecular calculations. *Computer Physics Reports* **1985**, *2*, 281-339.
12. Grimme, S., Semiempirical GGA-type density functional constructed with a long-range dispersion correction. *J. Comput. Chem.* **2006**, *27*, 1787-1799.
13. Liu, B.; Fang, Y.; Xia, W.; Terano, M., Theoretical investigation of novel silsesquioxane-supported Phillips-type catalyst by density functional theory (DFT) method. *Kinet. Catal.* **2006**, *47*, 234-240.